This is a peer-reviewed, accepted author manuscript of the following research article: Mularski, J & Li, J 2024, 'Assessment of biomass ignition potential and behavior using a cost-effective CFD approach', Fuel, vol. 361, 130637. https://doi.org/10.1016/j.fuel.2023.130637

Assessment of biomass ignition potential and behavior using a cost-effective CFD approach

Jakub Mularski [a, *], Jun Li [b, *]

[a] Faculty of Mechanical and Power Engineering, Wrocław University of Science and Technology, Wybrzeże Wyspiańskiego 27, 50-370, Poland

[b] Department of Chemical & Process Engineering, University of Strathclyde, James Weir Building, 75 Montrose Street, Glasgow, G1 1XJ, UK.

* Corresponding authors

phone: +48 71 320 41 52 (J. Mularski); +44 (0) 141 5482393 (J. Li)

email addresses: jakub.mularski@pwr.edu.pl, jun.li@strath.ac.uk

Abstract

This paper utilizes a CFD approach to study the ignition of pulverized biomass particles. Ignition is a critical parameter in a reactor's design and process efficiency, and a reliable and relatively quick method of its determination is a necessity. CFD is a well-established tool that has already proved credible in many combustion/gasification applications, and for that reason, its application in ignition-related studies should be paramount. In this research, an Eulerian-Lagrangian approach is used where key stages during biomass combustion such as inert heating, evaporation, devolatilization, gas-phase kinetics, char conversion, particle transport, and radiative transport are considered. The predictions of the model are verified against experimentally measured ignition data from the literature and are found to be in good agreement. The ignition delay is determined by monitoring the concentrations of OH (hydroxyl) and CH (methyl) radicals. It is concluded that using OH species as ignition indicator allowed reproducing the

delay better for lower temperatures, whereas, for temperatures above 1600K, CH species was found to be more accurate. The CFD approach was eventually found reasonable and relatively fast in ignition delay predictions enabling its wider use in industrial applications.

Keywords: Biomass ignition; CFD; Ignition delay; Combustion

Abbreviations

C2SM: Competing two step reaction model (Kobayashi model)

CFD: Computational Fluid Dynamics

DAE: Distributed Activation Energy

DAF: Dry-ash-free

DNS: Direct Numerical Simulation

DO: Discrete ordinate method

Nomenclature

A: Pre-exponential factor (unit depends on the reaction order)

A_0 – particle external surface area (m^2)

A_p: particle surface area (m^2)

C_D: drag coefficient (-)

C_1 – an overall mass diffusion-limited constant (the default value: $5 \cdot 10^{-12}$ $sK^{-0.75}$)

c_p: specific heat (J/kg K)

D_i: mass diffusion coefficient of species i (m^2/s)

d_p – particle diameter (m)

E: Activation Energy (J/ mol)

g: gravitational acceleration (m/s^2)

G – incident radiation (W/m^2)

h: coefficient of convective heat transfer (W/m^2K)

Δh_{evap}: enthalpy of evaporation (J/kg)

Δh_{devot}: enthalpy of devolatilization (J/kg)

Δh_{het}: enthalpy from heterogeneous reactions (J/kg)

h_{fg} – latent heat (J/kg)

$H_{C-O_2}, H_{C-CO_2}, H_{C-H_2O}$ – heat from the surface reactions (J/kg)

I – radiation intensity

k_a – absorption coefficient (1/m)

N_p – number of particles (-)

$\hat{n}$ – normal vector to the surface (-)

P – pressure (Pa)

Q_G- in the energy equation in the particle phase, it is heat from surface reactions (during particle surface combustion) and heat of vaporization (during particle evaporation)

R_j – rate of creation/destruction of species from surface reactions (kg/s)

s – beam direction considering radiation (-)

Sh: Sherwood number (-)

$S_{p,Y}$: source term due to inter-phase exchange in species(kg/$m^3 s$)

$S_{p,mom}$: inter-phase exchange term for momentum (kg/$m^2 s^2$)

$S_{p,m}$: inter-phase exchange term for mass (kg/$m^3 s$)

$S_{p,h}$: inter-phase exchange term for energy(kg/ms^3)

S_{rad}: source term due to radiation in gas-phase energy equation (kg/ms^3)

S_h: source term due to homogeneous reactions in gas-phase energy equation (kg/ms^3)

T – gas temperature (K)

T_p – particle temperature (K)

v: gas velocity (m/s)

v_p – particle velocity (m/s)

V_{cell} – cell volume (m^3)

Y – local mass fraction of the species (-)

Greek nomenclature

α_1: final volatile yield at low temperatures (-)

α_2: final volatile yield at high temperatures (-)

λ: thermal conductivity (W/m K)

δ_{ij}: Kronecker delta

μ: dynamic viscosity (kg/m s)

ρ – gas density (kg/m^3)

ρ_p – particle density (kg/m^3)

σ: Stefan-Boltzmann constant (W/$m^2\ K^4$)

η_r – the effectiveness factor (-)

1. Introduction

Ignition of biomass is a key parameter for a reactor's design, determining its optimum and safe operation, but also critical for fuel storage, transport, and handling, as biomass fuels tend to exhibit a high inclination toward self-heating, and consequently, self-ignition [1–3]. With respect to the reactors' operation, effective ignition can directly affect flame stability, pollutant formation, and combustion efficiency. However, ignition parameters such as ignition delay, ignition temperature, or ignition mechanism strongly depend on the fuel properties and the operating reactor's conditions thus making them extremely difficult to correctly predict [4]. Moreover, there is still no consensus concerning the criteria for identifying the moment of ignition. Research attempts have been made to experimentally define the moment of ignition in terms of the visible light signal [5–8], chemiluminescence emission [9,10], or OH- radicals [11,12]. Numerically, the moment of ignition was often defined with regard to CH or CO mass fractions [13], partial derivatives of gas and particle temperatures with respect to time [14], OH mass fraction [15], and a specific threshold of volatiles evolved [16]. It was reported that ignition delay can be evaluated based on the percentage loss of carbon and volatiles during combustion[17]. As a result, one can observe that such divergent measurement methods make it extremely difficult to standardize the ignition characteristics, and still more research is required in this field. In general, the ignition of solid fuels can be divided into three categories: (a) homogeneous ignition, where volatiles

ignite around the particle as oxidizer does not reach the particle surface; (b) heterogeneous ignition, where the particle is directly exposed to and in contact with oxidizer; and (c) hetero-homogeneous ignition, where ignition takes place simultaneously in the surrounding gas and at the particle surface. High-volatile coals and biomass fuels usually undergo homogeneous ignition, whereas low-volatile coals, chars, and metals mostly undergo heterogeneous ignition. In biomass homogeneous ignition, inert heating, evaporation, and devolatilization are mostly impactful combustion sub-stages. The particle's heat capacity, density, size, and shape would determine the rate of initial inert heating. There are two general modeling approaches of inert heating that have been reported. The first approach assumes the particle to be spherical and isothermal. An isotherm assumption is generally valid for low Biot numbers and pulverized particles. The second approach considers thermal gradients within particles [18], which should be applicable for particles larger than 200-300 μm [19]. In reality, the particle's morphological structure affects the rate at which water droplets migrate to the particle surface. Nowadays, evaporation is assumed to take place at the particle surface neglecting the morphology. There are several one-step models applied in the literature: the heat flux model [19,20], the equilibrium model [21], and the chemical reaction model [21]. In the heat flux model, the evaporation process is governed by the heat transfer to the particle, along with mass transfer inside the particle. In the chemical reaction model, the drying rate is described as a temperature-dependent Arrhenius relation. The rate of devolatilization and the yielding instantaneous species consisting of a mixture of CO, H_2, H_2O, hydrocarbons, tars with some other residuals, and the simultaneously occurring gas-phase reactions ultimately affect the occurrence of a homogeneous ignition. Currently, biomass devolatilization is commonly modeled as the weighted sum of the reference components (cellulose, hemicellulose, lignin) [22] where a hypothesis of non-interaction between them is generally assumed.

The commonly utilized biomass devolatilization models consist of global and detailed approaches. The global approaches, such as SFOR [23–26], C2SM [25], or DAE model [27], are easy to implement and have an associated reduced computational cost. The detailed approaches, such as FG-DVC [28] /FG-Biomass [29], Bio-CPD [30,31], Bio-Flashchain [32–35], and the Ranzi's mechanism [36–38], are much more complex in nature as they refer directly the fuel structure. The effect of devolatilization models was found to be essential in ignition delay studies [14]. Apart from devolatilization, the impact of gas-phase modeling was also found to be important in evaluating the ignition characteristics [14]. The most popular approaches involve one-point statistics with the application of PDF function, geometrical analysis with

flamelet assumptions, and turbulent mixing, where either global reactions or radical mechanisms, such as GRI-Mech [39] and CRECK [40–43] are utilized [44].

The rate and magnitude of all the above-mentioned combustion stages are additionally governed by the heating rate. Therefore, for an accurate simulation of ignition-related combustion characteristics, a complex modeling framework is required that would thoroughly account for the kinetic and diffusion effects including most of the aforementioned combustion sub-stages [45].

The determination of ignition delay by experimental techniques is very often time-consuming and restricted by access to highly specialized facilities and equipment. Numerical simulations, which are commonly applied in the field of combustion/gasification of solid fuels [45–49], can offer a reliable and time-saving alternative. For example, Niksa [16] integrated the detailed bio-Flashchain (bio-FC) devolatilization model [35] and the carbon burnout kinetic model for oxidation (CBK/E) [50] to predict the ignition-related combustion characteristics of pulverized biomass. Fatehi et al. [13] developed a one-dimensional model to identify the ignition mechanism and ignition delay of pulverized biomass particles. Zhang et al. developed a transient ignition and combustion model and proposed new ignition criteria [51]. Flamelet-based models were also successfully employed in ignition studies by Refs. [52–55]. Rieth et al. [56,57] applied a first-of-its-kind carrier-phase direct numerical simulation (DNS) of biomass combustion in a turbulent mixing layer, to determine the devolatilization rate and ultimate products from primary devolatilization. Mularski et al. [58] developed a 0-D modeling framework of pulverized biomass ignition that considered devolatilization and gas-phase models. Goshayeshi and Sutherland investigated the effect of different devolatilization models and gas-phase mechanisms on ignition [14]. Li et al. [59] applied machine learning architectures to study ignition. All studies report an acceptable agreement as regards the ignition delay.

Most of the published papers that investigate ignition numerically are characterized either with simplified modeling methods or very complex tools such as LES or DNS. The aim of the current research is to utilize CFD modeling tools oriented toward ignition determination that would account for most of the phenomena occurring at the very first instances of combustion and which would be cost-effective allowing for a relatively fast determination of ignition characteristics.

2. Numerical modeling

2.1 Overview

This section presents the structure of the modeling framework that was used as part of the CFD software ANSYS Fluent 2023 [60] to study biomass ignition behavior. The key model assumption is that biomass ignition is homogeneous, particles are pulverized, and the flow is laminar. The ignition mode and particle size are dictated by the model sequentiality. In the CFD model, char conversion is set to occur only after devolatilization. It results in the model's inability to predict heterogeneous or homo-heterogeneous ignition, where particle surface ignites during or even before devolatilization. However, numerous studies have proven that pulverized biomass particles tend to ignite homogeneously [6,13,61]. The reason for studying only pulverized fuels is that for larger particle sizes, the sequentiality of the combustion sub-stages becomes invalid as the moisture release, devolatilization, and char conversion tend to occur simultaneously and simply overlap [13]. Moreover, for larger particles, intraparticle heat transfer becomes impactful and, as a result, one cannot assume uniform particle temperature. The model also assumes particles to be spherical. The literature indicates [13,61] that non-spherical particles have a much higher propensity to ignite heterogeneously than spherical ones. However, since the model cannot predict this kind of ignition mode, the effect of non-sphericity cannot be effectively investigated. The shape of particles might affect the initial heating and the resulting heating rate acting on a particle could affect the ignition delay, but these aspects will simply not be investigated in this research.

With respect to the numerical methods, the Direct Numerical Simulation (DNS) was solved on a 2D structured mesh applying a finite volume discretization approach. The numerical grid was 100 x 2000 cells. The pressure-based solver was used. The SIMPLE [62] algorithm was utilized for pressure-velocity coupling. The convective fluxes in transport equations and the pressure gradient were discretized with second-order upwind schemes. The cell-based weighted-sum of gray-gas (WSGG) model is used for the calculation of the gas absorption coefficient. More details can be found in [60].

2.2 Modelling framework

2.2.1 Gas phase

The general steady-state conservation equations in the Eulerian frame of reference for mass, momentum, energy, and for the species were solved for gas phase and laminar flow. They are as follows:

$$\frac{\partial}{\partial x_i}(\rho v_i) = S_{p,m} \tag{2.1}$$

$$\frac{\partial}{\partial x_i}(\rho v_i v_j) = \rho g_j - \frac{\partial P}{\partial x_j} + \frac{\partial}{\partial x_i}\left(\mu\left(\frac{\partial v_i}{\partial x_j} + \frac{\partial v_j}{\partial x_i} - \frac{2}{3}\delta_{ij}\frac{\partial v_k}{\partial x_k}\right)\right) + S_{p,mom} \tag{2.2}$$

$$\frac{\partial}{\partial x_i}(\rho c_p v_i T) = \frac{\partial}{\partial x_i}\left(\lambda\frac{\partial T}{\partial x_i}\right) + S_{rad} + S_h + S_{p,h} \tag{2.3}$$

$$\frac{\partial}{\partial x_i}(\rho v_i Y_j) = \frac{\partial}{\partial x_i}\left(\rho D_i\frac{\partial Y_j}{\partial x_i}\right) + R_j + S_{p,Y,j} \tag{2.4}$$

The coupling between radiation and energy equation is achieved at the boundaries of the domain. The incident heat flux is defined as:

$$q_{in} = \int I_{in} s \cdot \hat{n} d\Omega \tag{2.5}$$

Subsequently, the incident heat flux in Eq. (2.5) is added to the energy equation to the component S_{rad}. Radiation was modeled with the discrete ordinate method [60] solving additional transport equations for radiation intensity in eight beam directions. Incident radiation was defined as an integral of the radiation intensity over the solid angle. Particle emissivity was assumed as 0.9

2.2.2 Particle phase

Particle dynamics are modeled using a Lagrangian formulation where equations for trajectory, velocity, mass, and temperature are solved.

As regards particle phase conservation equations, the mass balance equation is as follows:

$$\frac{dm_p}{dt} = \frac{dm_{C-O_2}}{dt} + \frac{dm_{C-CO_2}}{dt} + \frac{dm_{C-H_2O}}{dt} + \frac{dm_{devol}}{dt} + \frac{dm_{evap}}{dt} \tag{2.6}$$

208 Where the change of mass of a particle is equal to the change of mass due to evaporation,
209 devolatilization and surface reactions.

210 The trajectories of the particles were computed by integrating the momentum equation:

$$\frac{dv_p}{dt} = F_D + F_g \tag{2.7}$$

211 Where F_D and F_g are the drag and gravity forces per unit particle mass. The final form of the equation
212 is as follows:

$$\frac{dv_p}{dt} = \frac{18\mu}{\rho_p d_p^2} \cdot \frac{C_D}{24} \cdot \frac{\rho d_p |v - v_p|}{\mu}(v - v_p) + \frac{g(\rho_p - \rho)}{\rho_p} \tag{2.8}$$

213 Heat transfer to the particle considers contributions from convection, radiation and the heat
214 consumed/released during e.g. inert heating, surface reactions or vaporization.

$$m_p c_p \frac{dT_p}{dt} = h_p A_0 (T - T_p) + \frac{\epsilon_p A_0}{4}(G - 4\sigma T_p^4) + Q_G \tag{2.9}$$

215

216 The heat transfer coefficient is evaluated using the Ranz and Marshall correlation [63].

$$Nu = \frac{hd_p}{k} = 2 + 0.6Re^{0.5}Pr^{0.33} \tag{2.10}$$

217 Heat from surface reactions Q_G is defined in the following way:

$$Q_G = \frac{dm_{C-O_2}}{dt}H_{C-O_2} + \frac{dm_{C-CO_2}}{dt}H_{C-CO_2} + \frac{dm_{C-H_2O}}{dt}H_{C-H_2O} \tag{2.11}$$

218 During vaporization heat Q_G is defined as follows:

$$Q_G = -\frac{dm_p}{dt}h_{fg} \tag{2.12}$$

219 During inert heating, the Q_G term is not present.

220 As regards the heat of biomass pyrolysis Q_G, this quantity depends strongly on feedstock type,
221 temperature ranges, and the extent of secondary reactions. As a result, accurate characterization of it
222 is difficult [64]. In fact, various inconsistent results have been reported ranging from exothermic to
223 endothermic values [64,65]. In our research, the application of heat of pyrolysis did not affect the

temperature field nor the ignition delay. As a result, it has been assumed that devolatilization neither consumes nor releases the heat of pyrolysis.

As regards the coupling between gas and the discrete phase, the particle-source-in-cell method [66] is applied to evaluate the source terms that model the interactions between the gas and solid phases. These inter-phase terms are denoted by $S_{p,m}$, $S_{p,mom}$, $S_{p,h}$ and $S_{p,Y,j}$. Two-way coupling is used.

The inter-phase mass source term is expressed as:

$$S_{p,m} = \frac{1}{V_{cell}} \sum_{i=1}^{N_p} \frac{dm_{p,i}}{dt} = \frac{1}{V_{cell}} \sum_{i=1}^{N_p} \left(\frac{dm_{p,i}}{dt}\right)^{Ev} + \left(\frac{dm_{p,i}}{dt}\right)^{Dev} + \left(\frac{dm_{p,i}}{dt}\right)^{Het} \quad (2.13)$$

The mass change between the cell exit and the cell entry appears in the continuity equation and as a source of chemical species: $S_{p,Y,j}$. The mass change is due to evaporation, devolatilization and heterogeneous reactions.

The inter-phase momentum exchange source is calculated by summing the change in momentum of each particle passing through a control volume:

$$S_{p,mom} = \frac{1}{V_{cell}} \sum_{i=1}^{N_p} F_{D,i} \Delta m_{p,i} \quad (2.14)$$

The inter-phase energy exchange source is defined as:

$$S_{p,h} = \frac{1}{V_{cell}} \left(\sum_{i=1}^{N_p} \frac{1}{\Delta t} \Delta m_{p,i} \left(-\Delta h_{evap} + \Delta h_{het}\right) - \sum_{i=1}^{N_p} \frac{1}{\Delta t} \left(m_{p,i,out} \int_{T_{ref}}^{T_{p,out}} c_p dT - m_{p,i,in} \int_{T_{ref}}^{T_{p,in}} c_p dT \right) \right) \quad (2.15)$$

2.2.3 Particle combustion modeling

In general, during the solid fuel conversion process, the particle phase continuously interacts with the gas phase. The gas-phase chemistry was considered by applying a detailed GRI-Mech 3.0 mechanism [39]. The radical reaction approach provides the formation rate of species, such as CH or OH, which have been widely employed as representatives of ignition indicators. As for the particle phase, because numerous studies have proven that the effect of char conversion on homogeneous ignition is negligible [55,67–69], in this research, so as not to substantially affect the computational effort, the basic kinetic-

245 diffusion model is applied [70]. The model was commonly used in both combustion and gasification
246 studies providing reasonable results [45].

247 The char conversion model is structured as follows:

248 Diffusion rate coefficient for the reaction *i* is given by:

$$D_{0,i} = C_1 \frac{\left[\frac{T_p + T}{2}\right]^{0.75}}{d_p} \tag{2.16}$$

249 The kinetic rate of reaction r is defined as:

$$R_{kin,i} = A T_p^{\beta}\, exp\left(-\frac{E}{R T_p}\right) \tag{2.17}$$

250 When the reaction order is equal to one, the char consumption rate takes the following form:

$$R_{j,i} = \frac{A_p \eta_i Y_j p_n}{\frac{1}{D_0} + \frac{1}{R_{kin}}} \tag{2.18}$$

251 One of the key parts of the investigation considers devolatilization as it is critical in homogeneous
252 ignition. In this research, two approaches were employed, namely the Ranzi's mechanism, and the
253 competing two-step reaction mechanism (C2SM). The Ranzi's model is based on the decomposition of
254 biomass components, with an assumption of the decomposition products being the superposition of
255 decomposition of lignin, cellulose, cellulose, including the contribution of extractives (tannins,
256 triglycerides). The scheme consists of more than 40 reactions and 30 species representing the gas and
257 tar species yield. On the other hand, the C2SM model is a global approach that is based on two parallel
258 reactions competing at different heating rates and producing volatiles and a carbonized residue. The
259 two reactions are as follows:

$$biomass \xrightarrow{k_1} (1 - \alpha_1) char + \alpha_1 volatiles \tag{2.19}$$

$$biomass \xrightarrow{k_2} (1 - \alpha_2) char + \alpha_2 volatiles \tag{2.20}$$

260

261 The volatile yield is expressed through 2.21 [71]:

$$V = \int_0^t \left(\alpha_1 k_1(\tau) + \alpha_2 k_2(\tau)\right) exp\left(-\int_0^\tau (k_1(T) + k_2(T))dT\right) d\tau \quad (2.21)$$

262

263 In order not to affect the computational cost, the Ranzi's mechanism was used independently of CFD
264 as a stand-alone model. But its results regarding the volatile yield and the volatiles release rate were
265 incorporated into the C2SM through an optimization procedure [46,49] – Fig. 1. The evaluation of kinetic
266 parameters is carried out through the minimization of the below objective function:

$$OF(A, E, \alpha_1, \alpha_2) = \frac{\sum_{j=1}^{N_{t,j}} \left(Y_{i,j}^{Ranzi} - Y_{i,j}^{C2SM}(A, E, \alpha_1, \alpha_2)\right)^2}{N_{t,i}\left(max\left(Y_{i,j}^{Ranzi}\right)\right)^2} \quad (2.22)$$

267 where: Y^{Ranzi} is the volatile yield from the Ranzi's mechanism, Y^{C2SM} is the volatile yield from the C2SM
268 model obtained from Eq. (2.21) and $N_{t,j}$ is the number of discrete time steps. Solution is obtained based
269 on Levenberg-Marquardt fitting routine. The results from the optimization procedure will be discussed in
270 detail in Section 3: Results and Discussion.

271

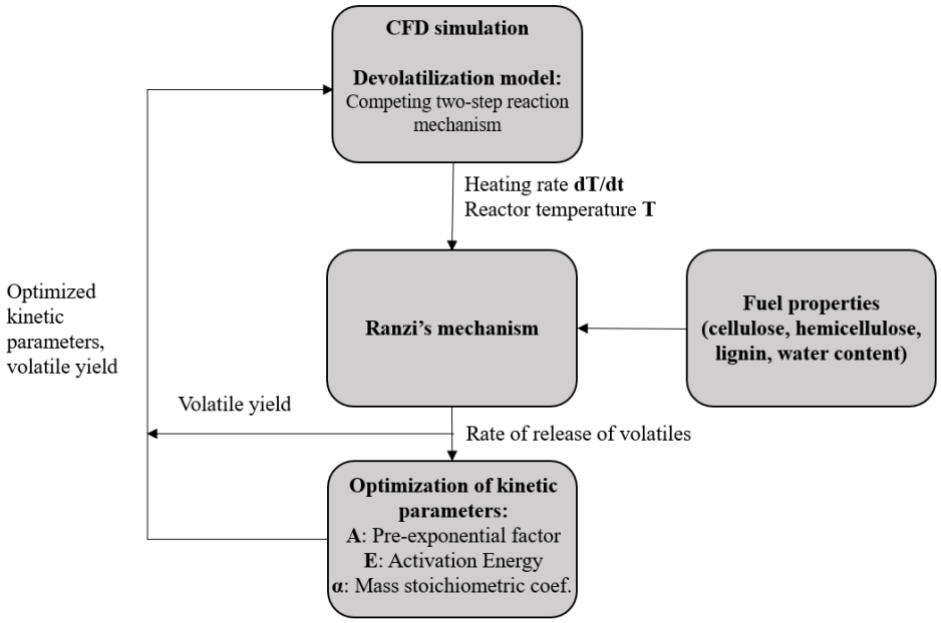

272

273 Fig. 1 Optimization procedure of C2SM model based on Ranzi's mechanism.

274

As regards the volatile matter, it was accounted for as a mixture of light gases and heavy hydrocarbons, which are released with a constant ratio during devolatilization. this assumption is not very accurate as, e.g., the release of tars takes place at lower temperatures, while light gases are released at higher temperatures. However, considering that the process was performed in high-heating rate conditions, with an equivalence ratio lower than 1, this assumption is feasible. In the real process, volatile matter yield is strongly dependent on the particle's heating rate. The higher the rate, the higher the yield of volatiles. The actual value of the volatile matter yield in given conditions compared to the volatile yield obtained from the proximate analysis is defined by the Q-factor. In this research, it is assumed that the fraction of volatiles in particles is constant, and it is defined a priori. As a result, the Q-factor is fixed and does not change during devolatilization. Since the focus of this study is ignition and the early phase of volatiles combustion, this assumption is believed acceptable.

The core idea of the iterative optimization procedure is illustrated in Fig. 1. It involves the following steps: at first, a CFD simulation is performed with literature-taken kinetic parameters. The procedure utilizes a particle heating rate from the CFD, which is expressed as a devolatilization-time-averaged heating rate, which is calculated as a ratio of the total change in temperature during the devolatilization process to its time of duration. Subsequently, based on biomass fuel properties, the detailed Ranzi's devolatilization mechanism predicts the rate of production and high-temperature yields of char, tar, volatiles, and their composition during devolatilization for the just calculated particle heating rate. In the subsequent step, the second CFD simulation is performed with optimized kinetic parameters for global models. The optimization is carried out through the minimization of the objective function – Eq. 2.22.

The overall structure of the CFD model is shown schematically in Fig. 2. For simplicity, the optimization procedure of devolatilization discussed just before was not included in this figure.

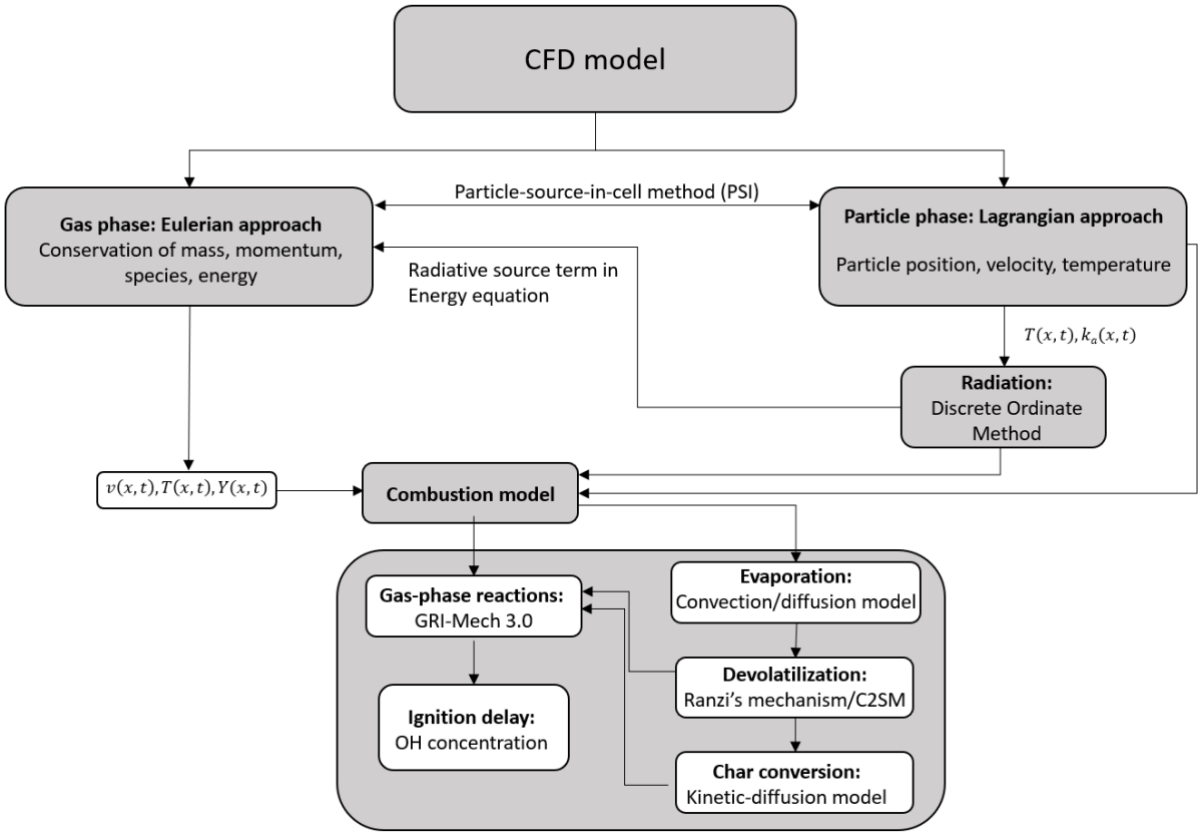

Fig. 2 CFD model

2.2.4 Material and Methodology

The CFD modeling was based on the experimental set-up described in detail in refs. [6,13,72]. A McKenna flat flame burner was the subject of investigation. A CH_4/air premixed flame produced a hot gas environment for the single particle biomass combustion. Biomass particle was transported by N_2 to the hot gas environment produced by the McKenna burner – Fig. 3. Ignition delay was studied experimentally at five reactor temperatures (1500, 1575, 1650, 1700, and 1800K) using a single particle combustion system where two particle size groups were investigated, 80-90 μm and 224-250 μm respectively. In their experiments, a CMOS high-speed camera was used to continuously record the ignition events. In this study, the investigation considered two fuels - pine bark and wheat straw that were studied in the reference experimental work. Their properties are presented in Table 1. It is worth

313 noting that pine bark has higher fixed carbon and moisture content and lower volatile matter content
314 than wheat straw. Moreover, pine bark has a lower oxygen content than wheat straw.

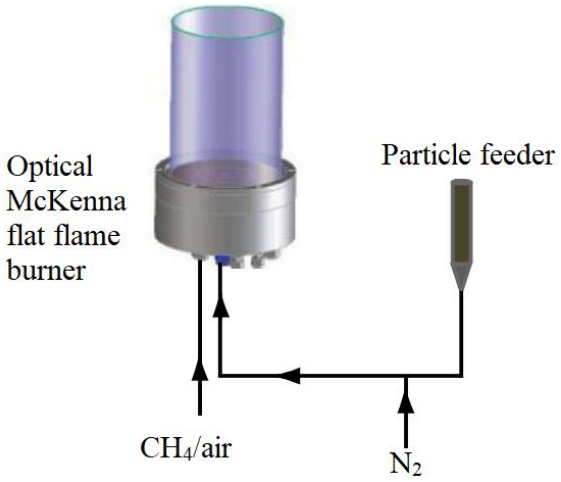

315

316 Fig. 3 Schematic view of literature experiment [6,13]

317

318 Table 1. Fuel properties and operating reactor conditions

	Pine bark [13]	**Wheat straw** [13]
C, daf	47.8	41.1
H, daf	4.3	5.3
O, daf	47.6	52.9
N, daf	0.3	0.7
S, daf	0	0
Volatile matter, ar	58.9	64.9
Fixed carbon, ar	25.9	11.5
Moisture, ar	13.9	8.9
Ash, ar	1.3	14.7
Temperature range [K] for reported Ignition tests	1500 -1800 [13]	1500 -1800 [13]

Particle size (μm)	80-230	80-230
Equivalence ratio [-]	0.7	0.7
LHV (MJ/kg)	17.1	13
Density (kg/m^3)	900	1100

319

320 ## 3. Results and discussion

321

322 ### 3.1 Optimization of devolatilization model

323 Fig. 4 depicts the volatile yield obtained from Ranzi's mechanism and the yields obtained from the C2SM
324 with both optimized and non-optimized kinetic parameters. Both sets of kinetic parameters before and
325 after optimization are shown in Table 2. By minimizing the objective function Eq. (2.17) one obtains
326 specific mass stoichiometric fractions, pre-exponential factors, and activation energies for the C2SM
327 model so that there is a minimum error between the volatile yield obtained by the Ranzi's mechanism
328 and the C2SM model. Ultimately, the goal is to mimic the behavior of the Ranzi's mechanism with C2SM
329 as regards the devolatilization rate. With respect to volatile composition, the yields of CH_4, CO, CO_2,
330 and H_2O used in the CFD model are the same as predicted from the Ranzi's model for the studied
331 reactor temperatures and heating rates.

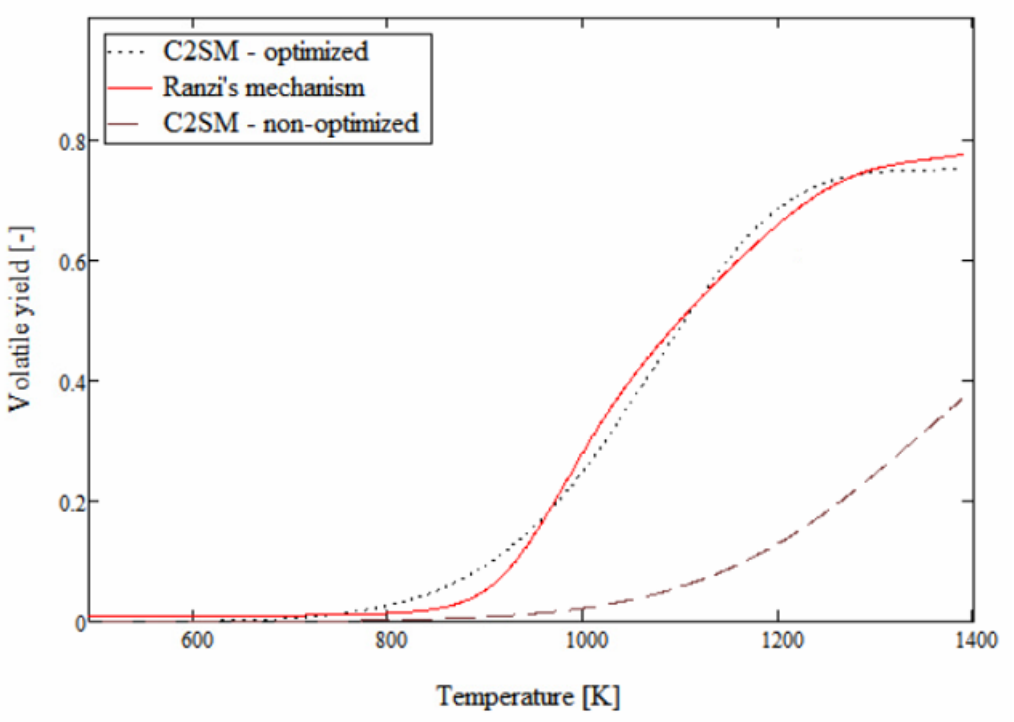

332

333 Fig. 4 Exemplary optimization of C2SM wheat straw volatile yield, based on the resultant species yield
334 from Ranzi's mechanism and the non-optimized model with literature parameters [73]

335

336 Table 2. Kinetic parameters for optimized and non-optimized C2SM

	Competing two-step reaction mechanism (C2SM)					
Parameters	α_1	α_2	A_1	A_2	E_1	E_2
	(-)	(-)	(1/s)	(1/s)	(J/kmol)	(J/kmol)
Non-optimized [60]	0.3	1	$2 \cdot 10^5$	$1.3 \cdot 10^7$	$1.046 \cdot 10^8$	$1.67 \cdot 10^8$
Optimized	0.5	0.752	100.2	$6.465 \cdot 10^6$	$1.137 \cdot 10^8$	$1.192 \cdot 10^8$

337

338 Table 3, on the other hand, illustrates the exemplary volatile composition of pine bark and wheat straw
339 that was obtained from the Ranzi's mechanism and which was further utilized in the CFD calculations
340 for a temperature of 1500K and 1800K. One can observe that for the given fuel, but for higher
341 temperatures, one obtains, more CO, less CO_2, and much more H_2 indicating that those volatiles at
342 higher temperatures will ignite faster. As regards the fuels, the key difference considers the amount of

343 H_2O indicating that wheat straw will most probably ignite faster. The exact ignition delay results will be
344 presented in Section 3.2.

345

346

347

348

349

350

351

352

353

354 Table 3. Exemplary volatile composition for pine bark and wheat straw for 1500K and 1800K

Species	**Pine bark – 1500K Mole fraction [%]**	**Pine bark – 1800K Mole fraction [%]**	**Wheat straw (WS) – 1500K Mole fraction [%]**	**Wheat straw (WS) – 1800K Mole fraction [%]**
CO	18	19	17	18.9
CO2	8.7	7.4	9.6	8.5
H2O	38.4	38.5	33.7	32.9
H2	0.8	5.4	0.9	6.2
CH4	3	4.6	2.3	4.2
C2H4	5.8	6.7	4.4	5.4
CH3OH	12.7	9.3	15.6	11.6
CH2O	12.7	9.4	16.5	12.2

355

3.2 Comparison of ignition indicators for predicting biomass ignition delay

The literature indicates that CH and OH radicals are the most commonly utilized species as ignition indicators for coal and biomass research [13,14,52,61]. However, there is still no common agreement as to which species yields the most accurate numerical ignition data with respect to experimental measurements. In this research, both species were compared in terms of ignition prediction. The results suggest that both radicals yield accurate results, although the OH species is more accurate at lower temperatures, whereas the CH species is more accurate at higher temperatures. Fig. 5 and Fig. 6 present experimental ignition delays that were measured in [6,13,72] – “Exp” and CFD model results from this research for wheat straw and pine bark (fuels from Table 1) for particle size of 80 microns. One can observe that for temperatures 1500 and 1570K, OH radical reproduces the experimental ignition delay results more accurately, whereas for temperatures 1650, 1700, and 1800K, CH radical is in better agreement with the experiment than OH. Of course, the agreement is not extreme and a slight discrepancy between the model and the experiment can be a result of the model simplifications. First of all, the simulation is steady-state, and two-dimensional. The transient effects are not fully accounted for. The particles are homogeneous spheres, whereas those in the experiment were slightly elongated with an aspect ratio higher than 1. Moreover, the CFD model considers in this case one specific particle size which is 80 microns. In the experiment, the particle size was in the range of 80-90 microns so the exact size was not known. However considering the relatively low-cost CFD model, the obtained agreement is reasonable.

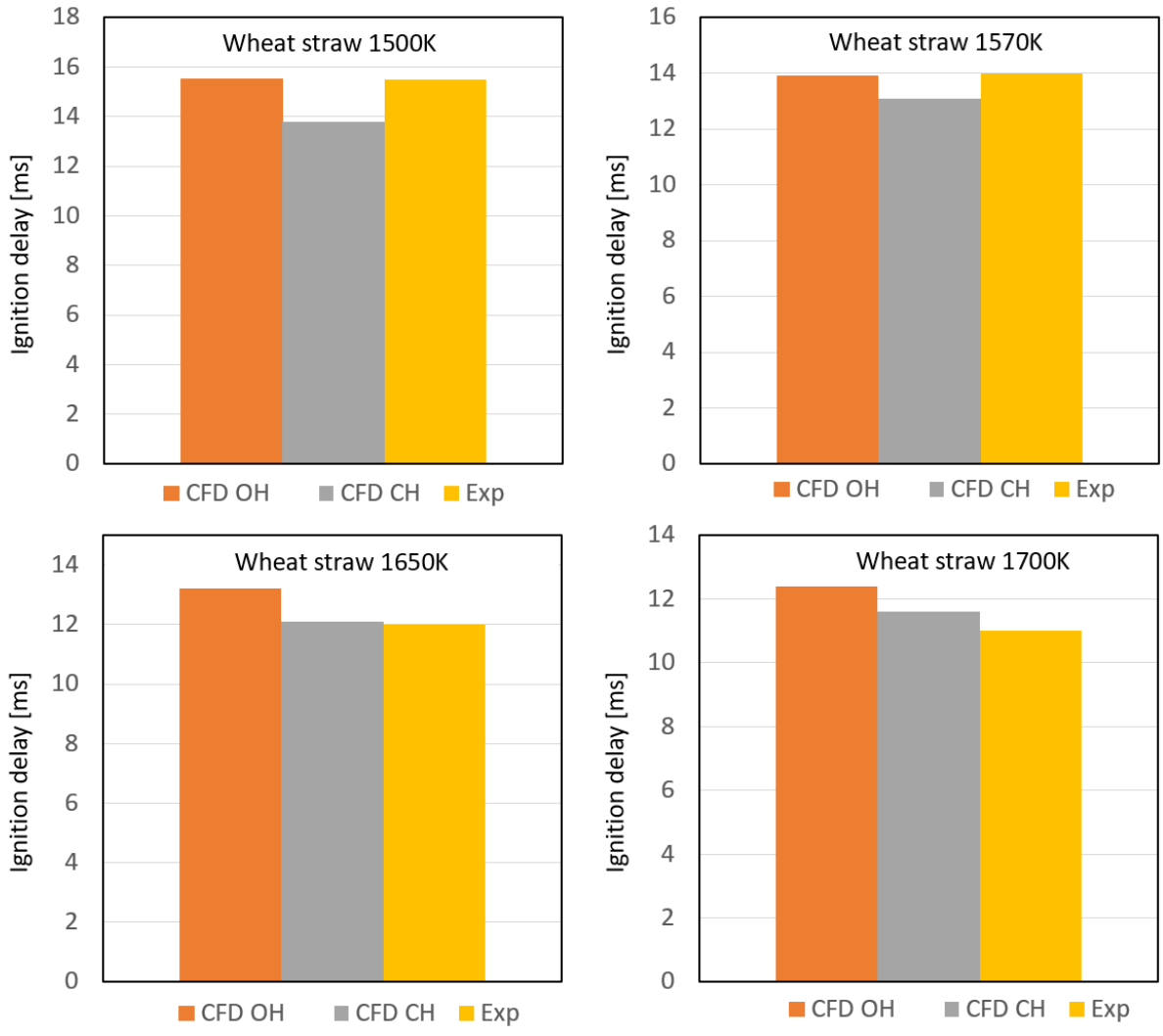

379

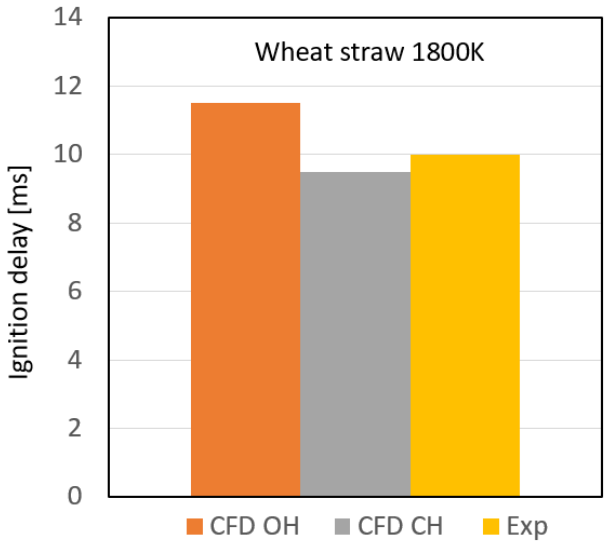

380

381 Fig. 5 Ignition delays of wheat straw measured as peaks in CH, OH, mass fractions with respect to

382 experimental data [13] for 1500-1800K.

383

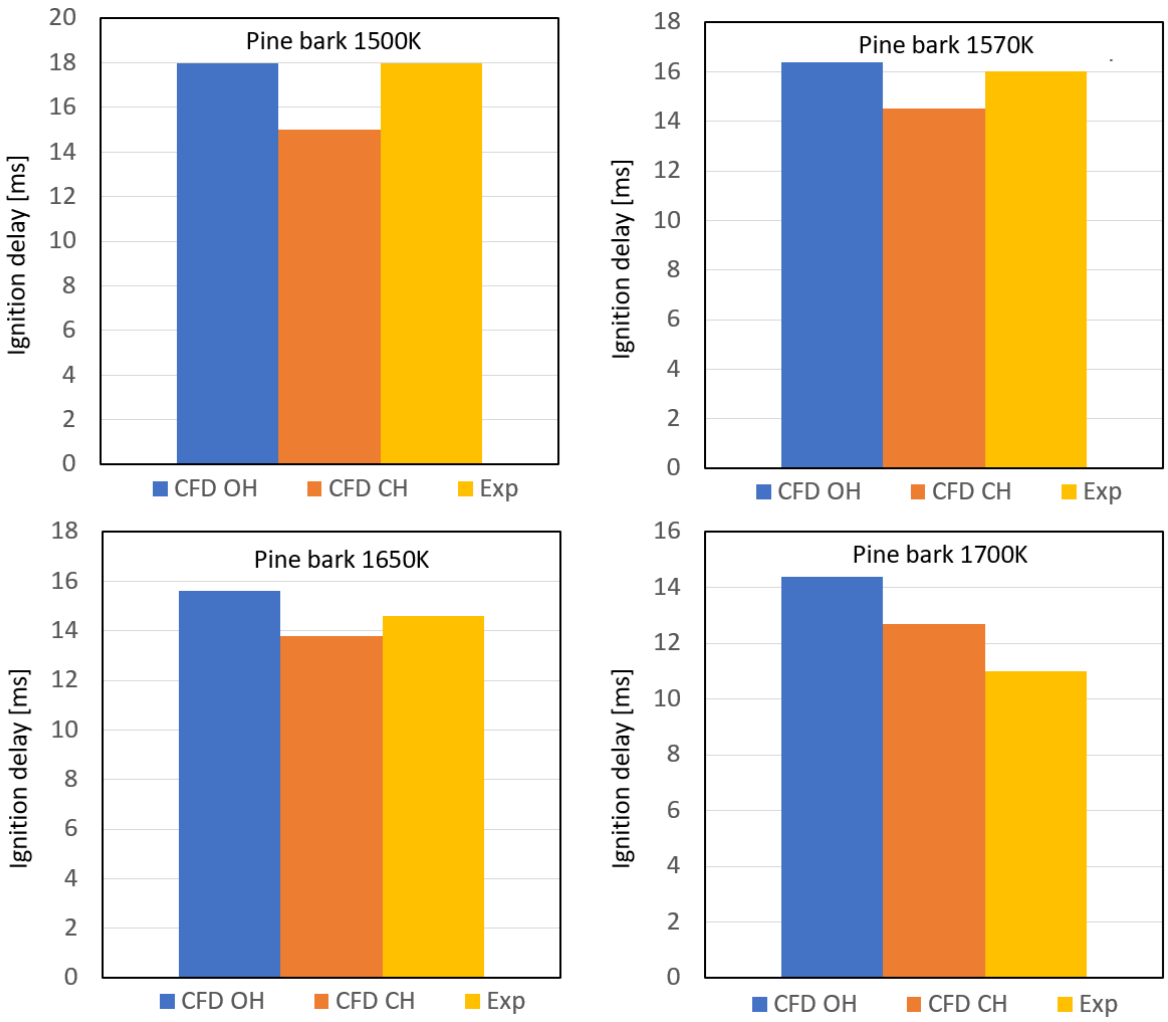

384

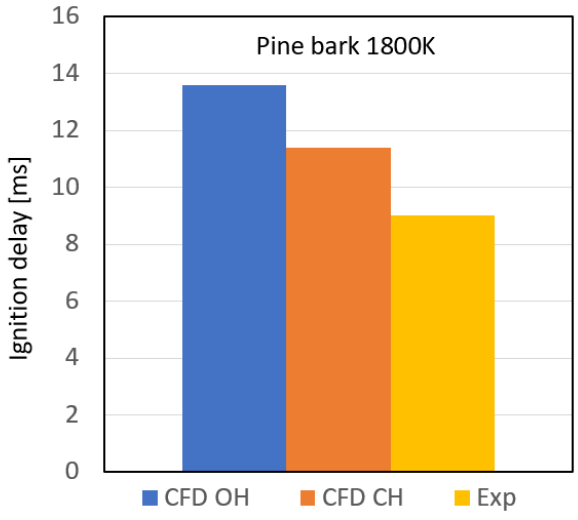

385

386 Fig. 6 Ignition delays of pine bark measured as peaks in CH, OH, mass fractions with respect to

387 experimental data [13] for 1500-1800K.

Fig. 7 illustrates the trend in ignition delay predictions by the CFD model from Fig. 5 and Fig. 6 but at a wider range of temperatures with OH and CH as ignition indicators. It is clear that the obtained trends for both CH and OH are reasonable and are close to the experimental values. Eventually, the research results suggest that in order to improve the accuracy of ignition delay evaluation, it is advisable to utilize both species as ignition indicators.

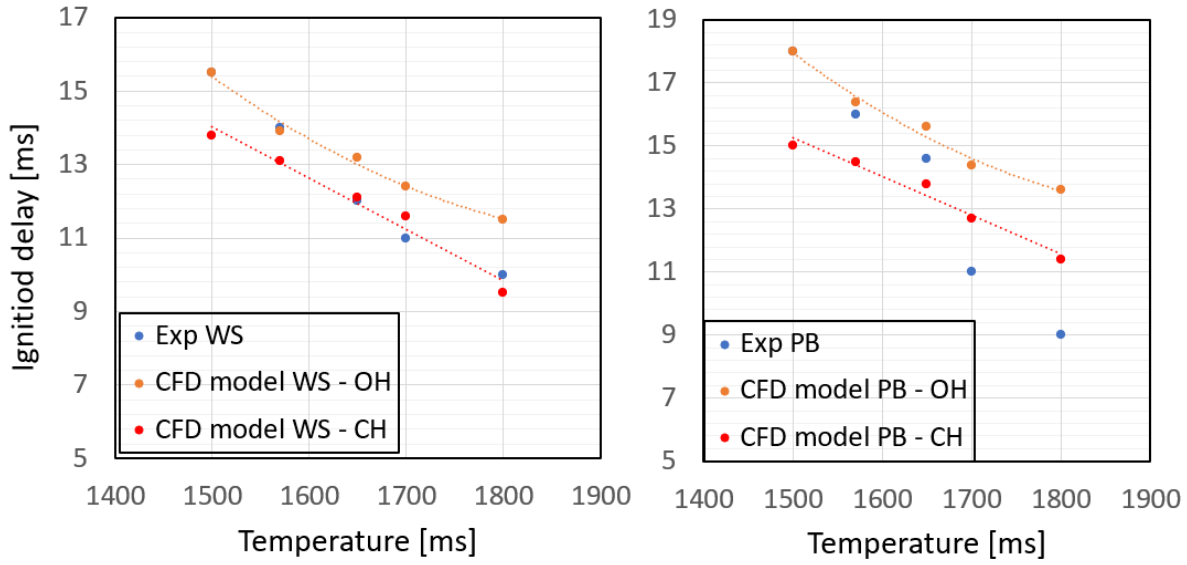

Fig. 7 Ignition delays of pine bark and wheat straw measured as peaks in OH and CH, mass fractions with respect to experimental data [13] for 1500-1800K.

3.3 Impact of particle size

Particle size is known to have a significant impact on the ignition delay [6,13]. However, its quantitative description has been so far challenging. The developed CFD approach has the capability of correctly predicting the effect of particle size on the ignition delay. Fig. 8 illustrates experimental [13] and CFD results of ignition delay of pine bark for reactor temperature of 1500 K and particle sizes of 80, 90, and 230 microns using OH as ignition indicator. One can observe an increasing ignition delay trend with increasing particle sizes for 80, 90, and 230 microns, respectively. Eventually, the numerical ignition delay of pine bark particle size 230 microns is confronted with experimentally measured ignition delay.

A reasonable agreement can be noticed between the model and the experiment. The difference is equal to 5.8 ms which is less than 20% of the experimentally obtained delay.

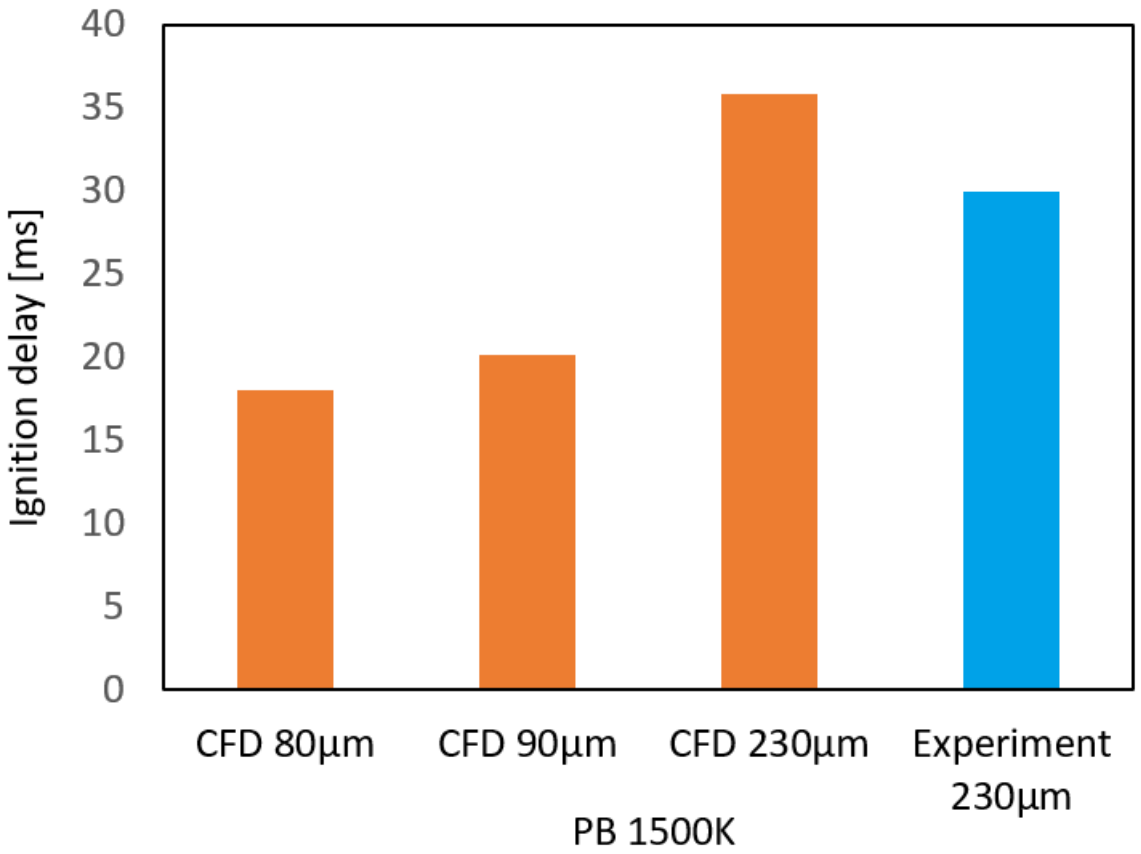

Fig. 8 Numerical ignition delays of pine bark for reactor temperature 1500K and for particle sizes of 80, 90, and 230 microns and experimental of particle size 230 microns [13]

3.4 Impact of moisture

Apart from particle size, the moisture content is the second key property that has an impact on ignition [13,61]. Biomass fuels tend to have high amount of moisture which reduces the gas temperature eventually affecting the initial particle heating rate and ignition. For example, for particle sizes larger than 250 microns, the drying time was found to be the controlling parameter in ignition delay time indicating an overlap between drying and devolatilization [74]. For high moisture content fuels, which are of pulverized size, even if the sequentiality of such processes as inert heating, evaporation, and devolatilization in numerical modeling is assumed, drying can still be the key step in the ignition onset

421 evaluation [74]. Fig. 9 presents the particle temperature of pine bark for a reactor temperature of 1500K
422 for four moisture contents: 2%, 10%, 15%, and 20%. A considerable effect of moisture content on the
423 particle temperature can be noticed. At 10 ms, particle temperature for a 20% moisture-content particle
424 is less than 373K, while for a 2% moisture-content particle it is around 600K. As a result, moisture
425 content has a key effect on ignition which can be seen in Fig. 9 where CFD modeling results of ignition
426 characteristics are confronted. Based on Figs. 9 and 10, ignition temperatures are in the range of 600 –
427 800K. Fig. 11 illustrates volatile evolution with respect to time. Although the rate of release is almost the
428 same for each moisture-content biomass fuel, it is the onset of devolatilization that differs in each case.

429

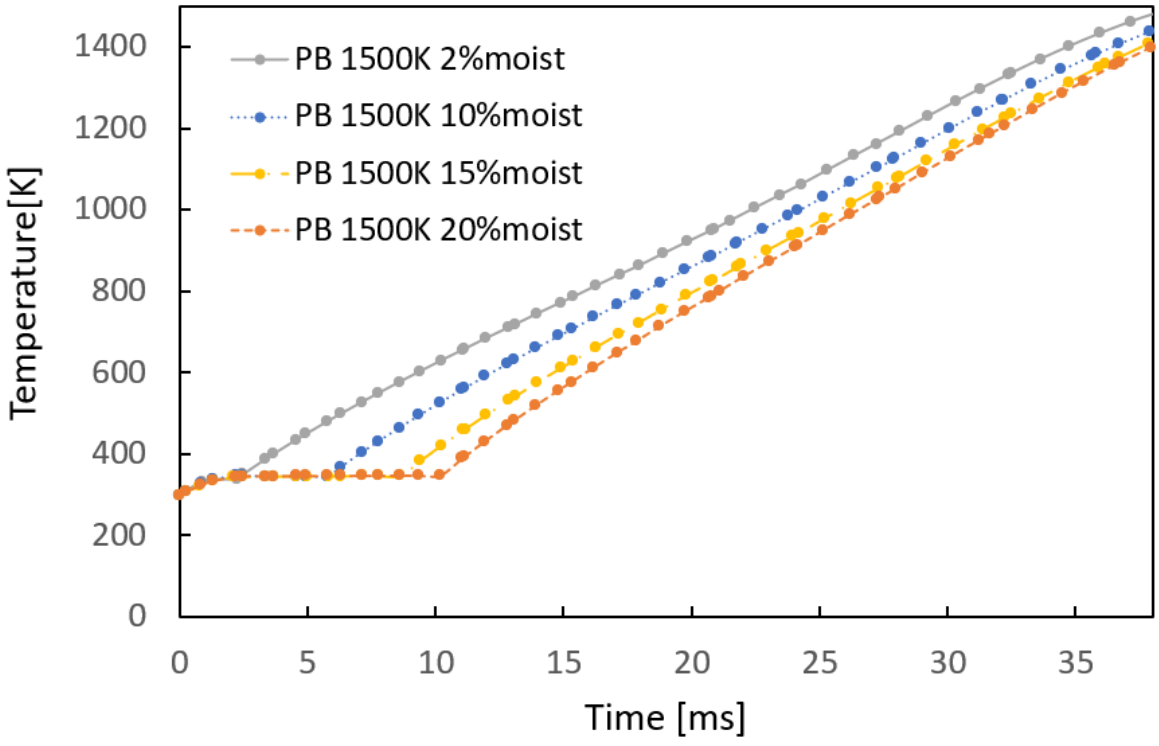

430

431 Fig. 9 Particle temperature for pine bark for reactor temperature 1500K for particle size 80 microns

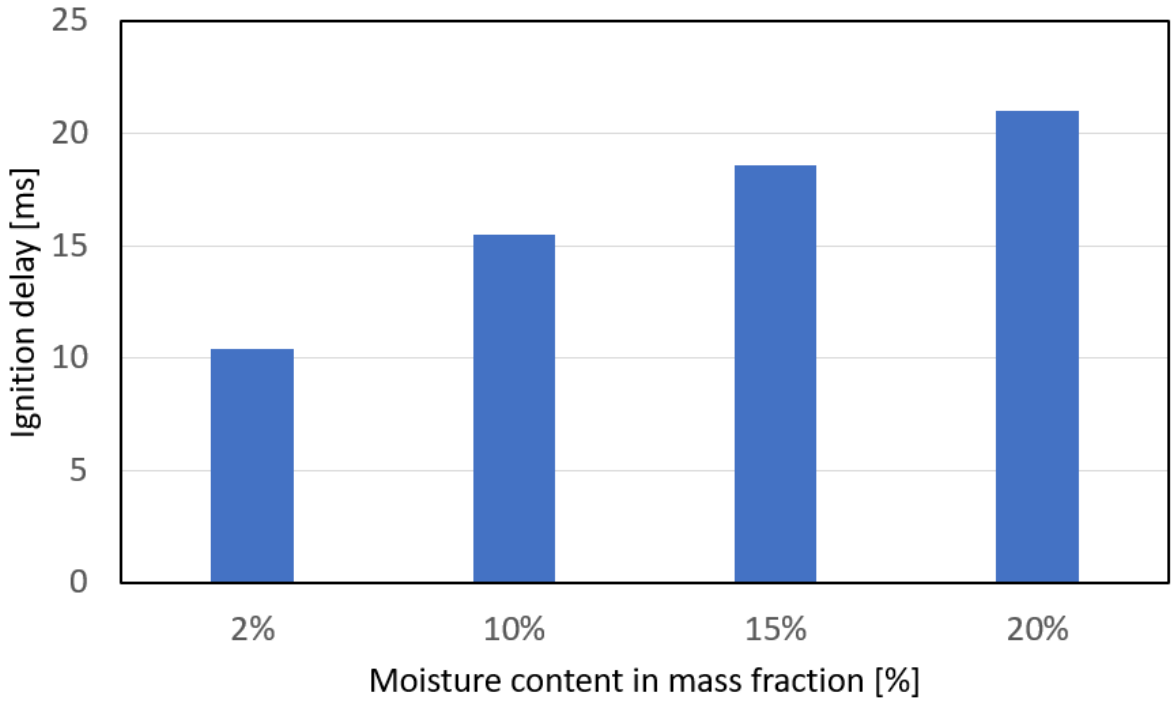

Fig. 10 Ignition delay of pine bark for reactor temperature 1500K, particle size 80 microns for four moisture contents (2%, 10%, 15%, 20%)

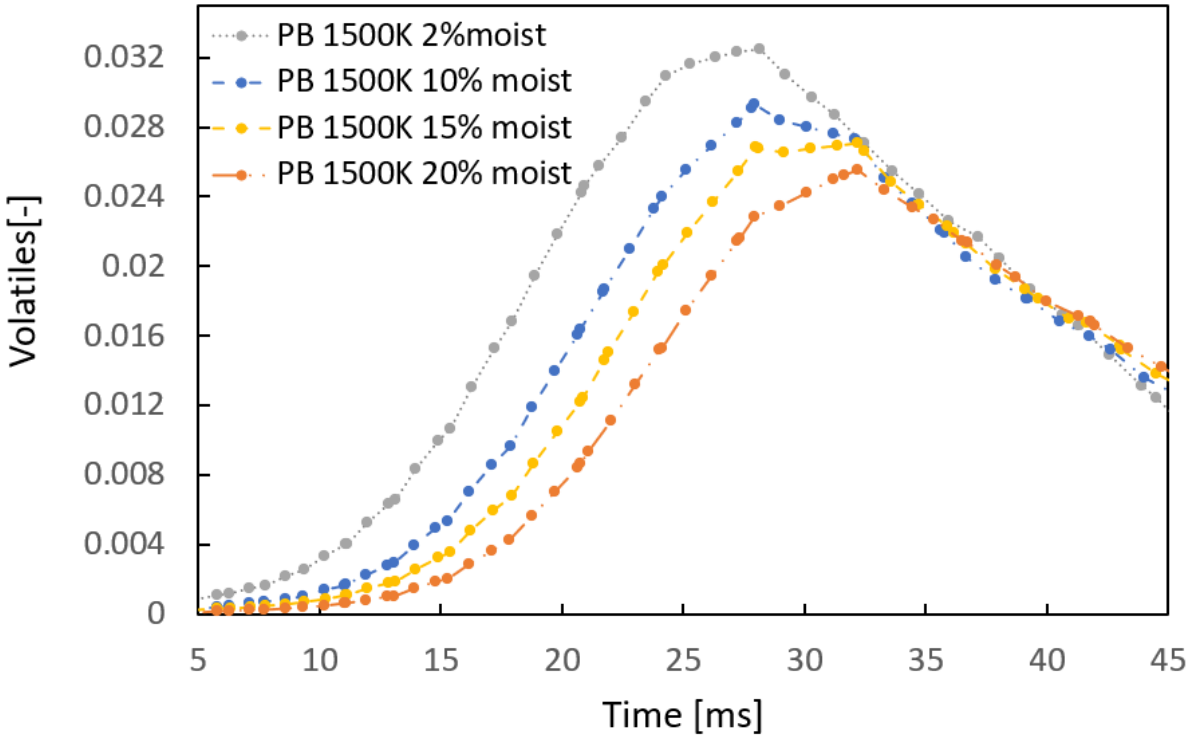

Fig. 11 Volatile release of pine bark for reactor temperature 1500K, particle size 80 microns for four moisture contents (2%, 10%, 15%, 20%).

4. Conclusions

The focus of the current research was to establish a cost-effective CFD model that could reasonably and relatively fast determine the ignition delay of different biomass fuels. The following conclusions can be drawn from the paper:

- The established CFD model reasonably predicted the ignition delay of pine bark and wheat straw for all investigated reactor temperatures (1500K, 1570K, 1600K, 1700K, 1800K) for different particle sizes (80 µm, 230 µm)
- It was observed that OH radicals used as an ignition indicator provided better accuracy of ignition delay for lower reactor temperatures (1500K, 1570K), whereas CH radicals were in better agreement with the experiment for higher reactor temperatures (1600K, 1700K, 1800K).
- The model reasonably predicted the increase in ignition delay for biomass particles with a higher moisture content although no experimental results were available to confront it.

Biomass ignition properties are critical with respect to fuel processing, safety issues, reactor operation, and process efficiency. The established CFD model with the developed optimization procedure should be of utility when investigating pulverized biomass fuels that tend to ignite homogeneously in laminar flow conditions both experimentally and numerically. The key effect of CH and OH radical species that was observed in this study, should be further analyzed in different operating reactor conditions.

Future work will be focused on the analysis of the effect of turbulence and the model upgrade to account for heterogeneous or hetero-homogeneous ignition modes. The role of CH and OH radical species will be further investigated.

References

[1] Garcia Torrent J, Fernandez Anez N, Medic Pejic L, Montenegro Mateos L. Assessment of self-ignition risks of solid biofuels by thermal analysis. Fuel 2015;143:484–91. https://doi.org/10.1016/j.fuel.2014.11.074.

[2] García Torrent J, Ramírez-Gómez Á, Fernandez-Anez N, Medic Pejic L, Tascón A. Influence of the composition of solid biomass in the flammability and susceptibility to spontaneous combustion. Fuel 2016;184:503–11. https://doi.org/10.1016/j.fuel.2016.07.045.

[3] Ramírez Á, García-Torrent J, Tascón A. Experimental determination of self-heating and self-ignition risks associated with the dusts of agricultural materials commonly stored in silos. J Hazard Mater 2010;175:920–7. https://doi.org/10.1016/j.jhazmat.2009.10.096.

[4] Li J, Paul MC, Czajka KM. Studies of Ignition Behavior of Biomass Particles in a Down-Fire Reactor for Improving Co-firing Performance. Energy and Fuels 2016;30:5870–7. https://doi.org/10.1021/acs.energyfuels.6b01065.

[5] Levendis YA, Joshi K, Khatami R, Sarofim AF. Combustion behavior in air of single particles from three different coal ranks and from sugarcane bagasse. Combust Flame 2011;158:452–65. https://doi.org/10.1016/j.combustflame.2010.09.007.

[6] Simões G, Magalhães D, Rabaçal M, Costa M. Effect of gas temperature and oxygen concentration on single particle ignition behavior of biomass fuels. Proc Combust Inst 2017;36:2235–42. https://doi.org/10.1016/j.proci.2016.06.102.

[7] Riaza J, Khatami R, Levendis YA, Álvarez L, Gil M V., Pevida C, et al. Combustion of single biomass particles in air and in oxy-fuel conditions. Biomass and Bioenergy 2014;64:162–74. https://doi.org/10.1016/j.biombioe.2014.03.018.

[8] Shaddix CR, Molina A. Particle imaging of ignition and devolatilization of pulverized coal during oxy-fuel combustion. Proc Combust Inst 2009;32 II:2091–8. https://doi.org/10.1016/j.proci.2008.06.157.

[9] Molina A, Shaddix CR. Ignition and devolatilization of pulverized bituminous coal particles during oxygen/carbon dioxide coal combustion. Proc Combust Inst 2007;31 II:1905–12. https://doi.org/10.1016/j.proci.2006.08.102.

[10] Yuan Y, Li S, Zhao F, Yao Q, Long MB. Characterization on hetero-homogeneous ignition of pulverized coal particle streams using CH∗chemiluminescence and 3 color pyrometry. Fuel 2016;184:1000–6. https://doi.org/10.1016/j.fuel.2015.11.032.

[11] Köser J, Becker LG, Vorobiev N, Schiemann M, Scherer V, Böhm B, et al. Characterization of single coal particle combustion within oxygen-enriched environments using high-speed OH-PLIF. Appl Phys B Lasers Opt 2015;121:459–64. https://doi.org/10.1007/s00340-015-6253-3.

[12] Köser J, Becker LG, Goßmann AK, Böhm B, Dreizler A. Investigation of ignition and volatile combustion of single coal particles within oxygen-enriched atmospheres using high-speed OH-PLIF. Proc Combust Inst

2017;36:2103–11. https://doi.org/10.1016/j.proci.2016.07.083.

[13] Fatehi H, Weng W, Costa M, Li Z, Rabaçal M, Aldén M, et al. Numerical simulation of ignition mode and ignition delay time of pulverized biomass particles. Combust Flame 2019;206:400–10. https://doi.org/10.1016/j.combustflame.2019.05.020.

[14] Goshayeshi B, Sutherland JC. A comparison of various models in predicting ignition delay in single-particle coal combustion. Combust Flame 2014;161:1900–10. https://doi.org/10.1016/j.combustflame.2014.01.010.

[15] Tufano GL, Stein OT, Wang B, Kronenburg A, Rieth M, Kempf AM. Coal particle volatile combustion and flame interaction. Part I: Characterization of transient and group effects. Fuel 2018;229:262–9. https://doi.org/10.1016/j.fuel.2018.02.105.

[16] Niksa S. Predicting the macroscopic combustion characteristics of diverse forms of biomass in p. p. firing. Fuel 2021;283:118911. https://doi.org/10.1016/j.fuel.2020.118911.

[17] Howard JB, Essenhigh RH. The mechanism of ignition of pulverized coal. Combust Flame 1965;9:337–9. https://doi.org/10.1016/0010-2180(65)90099-4.

[18] Yuen RKK, Yeoh GH, de Vahl Davis G, Leonardi E. Modelling the pyrolysis of wet wood - I. Three-dimensional formulation and analysis. Int J Heat Mass Transf 2007;50:4371–86. https://doi.org/10.1016/j.ijheatmasstransfer.2007.01.008.

[19] Yang YB, Sharifi VN, Swithenbank J, Ma L, Darvell LI, Jones JM, et al. Combustion of a single particle of biomass. Energy and Fuels 2008;22:306–16. https://doi.org/10.1021/ef700305r.

[20] Bruch C, Peters B, Nussbaumer T. Modelling wood combustion under fixed bed conditions. Fuel 2003;82:729–38. https://doi.org/10.1016/S0016-2361(02)00296-X.

[21] Lu H, Robert W, Peirce G, Ripa B, Baxter LL. Comprehensive study of biomass particle combustion. Energy and Fuels 2008;22:2826–39. https://doi.org/10.1021/ef800006z.

[22] Rabacal M, Costa M, Vascellari M, Hasse C. Kinetic modelling of sawdust and beech wood pyrolysis in drop tube reactors using advanced predictive models. Chem Eng Trans 2014;37:79–84. https://doi.org/10.3303/CET1437014.

[23] Badzioch S, Hawksley P. Kinetics of thermal decomposition of pulverized coal particles. Ind Eng Chem Process Des Dev 1970;9:521–30. https://doi.org/10.1021/i260036a005.

[24] Anthony DB, Howard JB, Hottel HC, Meissner HP. Rapid devolatilization of pulverized coal. Symp Combust 1975;15:1303–17. https://doi.org/10.1016/S0082-0784(75)80392-4.

[25] Kobayashi H, Howard JB, Sarofim AF. Coal devolatilization at high temperatures. Symp Combust

1977;16:411–25. https://doi.org/10.1016/S0082-0784(77)80341-X.

[26] Solomon PR, Colket MB. Coal devolatilization. Symp Combust 1979;17:131–43. https://doi.org/10.1016/S0082-0784(79)80016-8.

[27] Perkins G. Underground coal gasification – Part II: Fundamental phenomena and modeling. Prog Energy Combust Sci 2018;67:234–74. https://doi.org/10.1016/j.pecs.2018.03.002.

[28] Solomon PR, Hamblen DG, Carangelo RM, Serio MA, Deshpande G V. General Model of Coal Devolatilization. ACS Div Fuel Chem Prepr 1987;32:83–98. https://doi.org/10.1021/ef00010a006.

[29] Chen Y, Charpenay S, Jensen A, Wójtowicz MA, Serio MA. Modeling of biomass pyrolysis kinetics. Symp Combust 1998;27:1327–34. https://doi.org/10.1016/S0082-0784(98)80537-7.

[30] Fletcher TH, Pond HR, Webster J, Wooters J, Baxter LL. Prediction of tar and light gas during pyrolysis of black liquor and biomass. Energy and Fuels 2012;26:3381–7. https://doi.org/10.1021/ef300574n.

[31] Fletcher TH. Review of 30 Years of Research Using the Chemical Percolation Devolatilization Model. Energy & Fuels 2019;33:12123–53. https://doi.org/10.1021/acs.energyfuels.9b02826.

[32] Niksa S. bio-FLASHCHAIN® theory for rapid devolatilization of biomass 1. Lignin devolatilization. Fuel 2020;263:116649. https://doi.org/10.1016/j.fuel.2019.116649.

[33] Niksa S. bio-FLASHCHAIN® theory for rapid devolatilization of biomass 2. Predicting total yields for torrefied woods. Fuel 2020;263:116645. https://doi.org/10.1016/j.fuel.2019.116645.

[34] Niksa S. bio-FLASHCHAIN® theory for rapid devolatilization of biomass 3. Predicting total yields for torrefied grasses and agricultural residues. Fuel 2020;263:116646. https://doi.org/10.1016/j.fuel.2019.116646.

[35] Niksa S. Predicting the rapid devolatilization of diverse forms of biomass with bio-FLASHCHAIN. Proc Combust Inst 2000;28:2727–33. https://doi.org/10.1016/S0082-0784(00)80693-1.

[36] Ranzi E, Cuoci A, Faravelli T, Frassoldati A, Migliavacca G, Pierucci S, et al. Chemical kinetics of biomass pyrolysis. Energy and Fuels 2008;22:4292–300. https://doi.org/10.1021/ef800551t.

[37] Corbetta M, Frassoldati A, Bennadji H, Smith K, Serapiglia MJ, Gauthier G, et al. Pyrolysis of centimeter-scale woody biomass particles: Kinetic modeling and experimental validation. Energy and Fuels 2014;28:3884–98. https://doi.org/10.1021/ef500525v.

[38] Debiagi PEA, Pecchi C, Gentile G, Frassoldati A, Cuoci A, Faravelli T, et al. Extractives Extend the Applicability of Multistep Kinetic Scheme of Biomass Pyrolysis. Energy and Fuels 2015;29:6544–55. https://doi.org/10.1021/acs.energyfuels.5b01753.

[39] Smith G, Golden D, Frenklach M, Moriarty N, Eiteneer B, Goldenberg M, et al. GRI-Mech 3.0 2000. http://combustion.berkeley.edu/gri-mech/version30/text30.html (accessed October 14, 2018).

[40] Ranzi E, Cavallotti C, Cuoci A, Frassoldati A, Pelucchi M, Faravelli T. New reaction classes in the kinetic modeling of low temperature oxidation of n-alkanes. Combust Flame 2015;162:1679–91. https://doi.org/10.1016/j.combustflame.2014.11.030.

[41] Ranzi E, Frassoldati A, Grana R, Cuoci A, Faravelli T, Kelley AP, et al. Hierarchical and comparative kinetic modeling of laminar flame speeds of hydrocarbon and oxygenated fuels. Prog Energy Combust Sci 2012;38:468–501. https://doi.org/10.1016/j.pecs.2012.03.004.

[42] Frassoldati A, Cuoci A, Faravelli T, Niemann U, Ranzi E, Seiser R, et al. An experimental and kinetic modeling study of n-propanol and iso-propanol combustion. Combust Flame 2010;157:2–16. https://doi.org/10.1016/j.combustflame.2009.09.002.

[43] Sommariva S, Maffei T, Migliavacca G, Faravelli T, Ranzi E. A predictive multi-step kinetic model of coal devolatilization. Fuel 2010;89:318–28. https://doi.org/10.1016/j.fuel.2009.07.023.

[44] Poinsot T, Veynante D. Theoretical and numerical combustion Third Edition 2012.

[45] Mularski J, Pawlak-Kruczek H, Modlinski N. A review of recent studies of the CFD modelling of coal gasification in entrained flow gasifiers, covering devolatilization, gas-phase reactions, surface reactions, models and kinetics. Fuel 2020;271:1–36. https://doi.org/10.1016/j.fuel.2020.117620.

[46] Mularski J, Modliński N. Entrained flow coal gasification process simulation with the emphasis on empirical devolatilization models optimization procedure. Appl Therm Eng 2020;175:1–14. https://doi.org/10.1016/j.applthermaleng.2020.115401.

[47] Hasse C, Debiagi P, Wen X, Hildebrandt K, Vascellari M, Faravelli T. Advanced modeling approaches for CFD simulations of coal combustion and gasification. Prog Energy Combust Sci 2021;86:100938. https://doi.org/10.1016/j.pecs.2021.100938.

[48] Mularski J, Modliński N. Impact of Chemistry–Turbulence Interaction Modeling Approach on the CFD Simulations of Entrained Flow Coal Gasification. Energies 2020;13:6467. https://doi.org/10.3390/en13236467.

[49] Mularski J, Modliński N. Entrained-Flow Coal Gasification Process Simulation with the Emphasis on Empirical Char Conversion Models Optimization Procedure. Energies 2021;14:1729. https://doi.org/10.3390/EN14061729.

[50] Niksa S, Liu GS, Hurt RH. Coal conversion submodels for design applications at elevated pressures. Part I. Devolatilization and char oxidation. Prog Energy Combust Sci 2003;29:425–77.

https://doi.org/10.1016/S0360-1285(03)00033-9.

[51] Zhang T, Hu Z, Zhou Y. The determination method of the ignition modes of single coal particle with a transient coal ignition and combustion model. Combust Flame 2022;241. https://doi.org/10.1016/j.combustflame.2022.112092.

[52] Vascellari M, Xu H, Hasse C. Flamelet modeling of coal particle ignition. Proc Combust Inst 2013;34:2445–52. https://doi.org/10.1016/j.proci.2012.06.152.

[53] Vascellari M, Tufano GL, Stein OT, Kronenburg A, Kempf AM, Scholtissek A, et al. A flamelet/progress variable approach for modeling coal particle ignition. Fuel 2017;201:29–38. https://doi.org/10.1016/j.fuel.2016.09.005.

[54] Knappstein R, Kuenne G, Meier T, Sadiki A, Janicka J. Evaluation of coal particle volatiles reaction by using detailed kinetics and FGM tabulated chemistry. Fuel 2017;201:39–52. https://doi.org/10.1016/j.fuel.2016.10.033.

[55] Farmand P, Nicolai H, Schumann C, Attili A, Berger L, Li T, et al. Numerical investigation and assessment of flamelet-based models for the prediction of pulverized solid fuel homogeneous ignition and combustion. Combust Flame 2022;235:111693. https://doi.org/10.1016/j.combustflame.2021.111693.

[56] Rieth M, Kempf AM, Kronenburg A, Stein OT. Carrier-phase DNS of pulverized coal particle ignition and volatile burning in a turbulent mixing layer. Fuel 2018;212:364–74. https://doi.org/10.1016/j.fuel.2017.09.096.

[57] Rieth M, Rabaçal M, Kempf AM, Kronenburg A, Stein OT. Carrier-Phase DNS of biomass particle ignition and volatile burning in a turbulent mixing layer. Chem Eng Trans 2018;65:37–42. https://doi.org/10.3303/CET1865007.

[58] Mularski J, Lue L, Li J. Development of a numerical method for the rapid prediction of ignition performance of biomass particles. Fuel 2023;348:128520. https://doi.org/10.1016/j.fuel.2023.128520.

[59] Li T, Liang Z, Dreizler A, Böhm B. Accurate determination of homogeneous ignition of single solid fuel particles enabled by machine learning. Fuel 2023;338:127171. https://doi.org/10.1016/j.fuel.2022.127171.

[60] Ansys inc. ANSYS Fluent Theory Guide. ANSYS Inc, USA 2022:995.

[61] Mularski J, Li J. A review on biomass ignition: Fundamental characteristics, measurements, and predictions. Fuel 2023;340:127526. https://doi.org/10.1016/j.fuel.2023.127526.

[62] Patankar S., Spalding D. A calculation procedure for heat, mass and momentum transfer in three-dimensional parabolic flows. Int J Heat Mass Transf 1972;15:1787–806. https://doi.org/10.1016/0017-

9310(72)90054-3.

[63] Ranz, W. E. and Marshall WR. Evaporation from Drops. Chem Eng Prog 1952;48:141–6.

[64] Chen Q, Yang R, Zhao B, Li Y, Wang S, Wu H, et al. Investigation of heat of biomass pyrolysis and secondary reactions by simultaneous thermogravimetry and differential scanning calorimetry. Fuel 2014;134:467–76. https://doi.org/10.1016/j.fuel.2014.05.092.

[65] Stenseng M, Jensen A, Dam-Johansen K. Investigation of biomass pyrolysis by thermogravimetric analysis and differential scanning calorimetry. J Anal Appl Pyrolysis 2001;58–59:765–80. https://doi.org/10.1016/S0165-2370(00)00200-X.

[66] Crowe C, Sharma MP, Stosk DE. The Particle-source-in Cell (PSI-CELL) Model for Gas-droplet Flows. J Fluids Eng 1977;99:392–332. https://doi.org/doi:10.1115/1.3448756.

[67] Farazi S, Attili A, Kang S, Pitsch H. Numerical study of coal particle ignition in air and oxy-atmosphere. Proc Combust Inst 2019;37:2867–74. https://doi.org/10.1016/j.proci.2018.07.002.

[68] Knappstein R, Kuenne G, Ketelheun A, Köser J, Becker L, Heuer S, et al. Devolatilization and volatiles reaction of individual coal particles in the context of FGM tabulated chemistry. Combust Flame 2016;169:72–84. https://doi.org/10.1016/j.combustflame.2016.04.014.

[69] Tufano GL, Stein OT, Kronenburg A, Frassoldati A, Faravelli T, Deng L, et al. Resolved flow simulation of pulverized coal particle devolatilization and ignition in air- and O2/CO2-atmospheres. Fuel 2016;186:285–92. https://doi.org/10.1016/j.fuel.2016.08.073.

[70] Smith IW. The combustion rates of coal chars: A review. Symp Combust 1982;19:1045–65. https://doi.org/10.1016/S0082-0784(82)80281-6.

[71] Ansys Fluent User guide n.d. https://www.sharcnet.ca/Software/Ansys/18.2.2/en-us/help/ai_sinfo/flu_intro.html (accessed March 9, 2019).

[72] Weng W, Costa M, Aldén M, Li Z. Single particle ignition and combustion of pulverized pine wood, wheat straw, rice husk and grape pomace. Proc Combust Inst 2019;37:2663–71. https://doi.org/10.1016/j.proci.2018.05.095.

[73] Ali M, Jahromi Y, Atashkari K, Kalteh M. Performance Evaluation of a Two-Stage Entrained-Flow Coal Gasifier Using Numerical Simulation. Chem Eng Technol 2020;43:1316–26. https://doi.org/10.1002/ceat.201900093.

[74] Fatehi H, Weng W, Li Z, Bai XS, Aldén M. Recent development in numerical simulations and experimental studies of biomass thermochemical conversion. Energy and Fuels 2021;35:6940–63.

647 https://doi.org/10.1021/acs.energyfuels.0c04139.

648